Traveling-Wave Tube Devices with Nonlinear Dielectric Elements

Thomas M. Antonsen, Jr., *Member, IEEE,* and Baruch Levush, *Senior Member, IEEE*

***Abstract*—The performance of traveling-wave tube (TWT) amplifiers incorporating nonlinear dielectric elements is studied via computer simulation. Two different situations are investigated: 1) the use of nonlinear dielectric elements to reduce intermodulation distortion and 2) the use of voltage-controlled dielectrics to provide rapid modification of the dispersion characteristics of the slow-wave structure. In the first case, the use of dielectrics with negative second-order susceptibilities is studied as a means of reducing phase and intermodulation distortion. Use of these dielectrics along with dynamic velocity taper to reduce amplitude modulation distortion results in marked reduction of predicted intermodulation distortion. In the second case, the goal is to design an amplifying structure whose gain as a function of frequency can be varied electrically. Preliminary design studies show that relatively large changes in the center frequency of the amplification band can be achieved with relatively modest changes in the dielectric constant of helix support structure.**

***Index Terms*— Electronic tuning, intermodulation distortion, nonlinear dielectric, traveling-wave amplifier.**

I. Introduction

IN MANY applications of traveling-wave tubes (TWT's) in the defense arena, including EW, radar, and communication applications, TWT amplifiers are required to provide simultaneous amplification of multiple frequencies. In these applications, intermodulation and amplitude and phase cross modulation will take place as a result of the nonlinearities in the amplification process. In cases when the number of carriers is large, this phenomenon becomes even more complex. In existing tubes, these parasitic effects are avoided by a combination of techniques such as feedforward compensation [1]–[3] or operation in the linear regime with depressed energy collection of the electron beam [4]. Associated with these techniques are the cost of increasing the complexity of the tube or weight of the power supply. Some EW applications require intermodulation products at levels of no greater than -30 to -40 dB·C and phase stability less than 3°/dB. Communication applications can require intermodulation levels as low as -70 dB·C. These levels can be achieved in narrow-band applications by a technique known as predistortion linearization [5], [6] in which the signal is deliberately distorted, prior to injection in the TWT, in such a away that the combination of the TWT and predistortion nonlinearities cancel. Alternately, some applications require amplifications of signals over a range in frequency which may exceed the range of optimal performance of the TWT. In this case, it would be beneficial to be able to control electrically the band-pass characteristics of the amplifier, so that it could adapt rapidly to the changing properties of the signal.

This paper investigates theoretically the possibility of achieving reduced distortion and dynamic tuning of TWT amplifiers using nonlinear dielectric elements. In the case of reducing distortion, the basic idea is that a nonlinear dielectric element in the signal path can introduce phase distortion which will cancel the phase distortion inherent in the amplification process. Such an element would be used in conjunction with a TWT which was designed to minimize amplitude distortion. This idea is similar to that of the predistortion linearizer [5], [6]. It has possible advantages over the predistortion linearizer in that the phase distortion can be introduced at the output of the amplifier. This results in a cancellation of distortion which is more complete over a greater range of operating powers and frequencies. It suffers from the disadvantage that the nonlinear elements are inserted in the highest power portion of the signal path, and thus, these elements must have low losses. In the second case, that of realizing an electrically controllable amplifier, we consider inserting nonlinear voltage-controlled dielectric elements in the support structures of the TWT helix. These elements then allow for varying of the phase velocity and impedance of the slow-wave structure and consequently tuning the amplification band of the TWT. In addition to varying the amplification band, such elements would allow one to electrical compensate for voltage fluctuations in the injected electron beam [7].

The organization of this paper is as follows. In Section II we present the theoretical model, describing multifrequency operation of a TWT, on which our subsequent calculations are based. Included in this section is a description of the way in which nonlinear dielectric elements in the circuit are modeled. Section III presents an example of the reduction of intermodulation distortion for an amplifier with a specific set of parameters. Section IV illustrates the way in which nonlinear dielectric elements can be used to control the frequency response of an amplifier. Finally, in Section V, we discuss some

Manuscript received September 19, 1997; revised January 7, 1998. This work was supported by the Office of Naval Research.

T. M. Antonsen, Jr. is with the Naval Research Laboratory, Washington, DC 20375-5320 USA. He is also with the Science Applications International Corporation, McLean, VA 22102, and the Departments of Electrical Engineering and Physics, University of Maryland, College Park, MD 20742 USA.

B. Levush is with the Vacuum Electronic Branch, Naval Research Laboratory, Washington, DC 20375-5320 USA.

Publisher Item Identifier S 0093-3813(98)04389-6.

of the issues surrounding the implementation of nonlinear dielectrics in these devices.

II. Physical Model

A. Electromagnetic Fields of the Structure and Their Frequencies

The physical model [8]–[17] employed in the current study is essentially the same as that used in the development of the one-dimensional (1-D) multifrequency simulation code CHRISTINE [8]. We begin the description of the physical model with the representation of the assumed fields of the cold structure. Ultimately, in the type of model presented here, only two frequency-dependent quantities, the phase velocity and the coupling impedance, are needed to specify the parameters of the cold structure fields. However, the presentation will start at a more basic level to underscore the nature of the approximations being made.

The fields of the structure are represented in the form of the product of a slowly varying complex amplitude δA_n, periodic eigenfunctions $\boldsymbol{e}_n(\boldsymbol{x})$ and $\boldsymbol{b}_n(\boldsymbol{x})$, and an exponential phase factor

$$\boldsymbol{E}_{rf}(x,t) = \sum_n i\frac{\omega_n}{c}\delta A_n(z)\boldsymbol{e}_n(\boldsymbol{x}) \cdot \exp\left[i\left(\int_0^z k_{zn}(z')\,dz' - \omega_n t\right)\right] + \text{c.c.} \tag{1a}$$

and

$$\boldsymbol{B}_{rf}(x,t) = \sum_n i\frac{\omega_n}{c}\delta A_n(z)\boldsymbol{b}_n(\boldsymbol{x}) \cdot \exp\left[i\left(\int_0^z k_{zn}(z')\,dz' - \omega_n t\right)\right] + \text{c.c.} \tag{1b}$$

Here it is assumed that $\boldsymbol{e}_n(\boldsymbol{x})$ and $\boldsymbol{b}_n(\boldsymbol{x})$ are the solutions of Maxwell's equations for the empty structure corresponding to angular frequency ω_n and real axial wavenumber k_{zn}. In this regard $\boldsymbol{e}_n(\boldsymbol{x})$ and $\boldsymbol{b}_n(\boldsymbol{x})$ will be periodic in axial distance with a period equal to that of the structure. To allow for the slow axial variation of parameters of the structure, the wavenumber k_{zn} corresponding to frequency ω_n as well as the eigensolutions $\boldsymbol{e}_n(\boldsymbol{x})$ and $\boldsymbol{b}_n(\boldsymbol{x})$ will vary with axial distance. It is assumed that such variations are slow and that it is permissible to think of the functions $\boldsymbol{e}_n(\boldsymbol{x})$ and $\boldsymbol{b}_n(\boldsymbol{x})$ as being locally periodic. As Maxwell's equations for the cold structure are linear, we can take the eigensolutions $\boldsymbol{e}_n(\boldsymbol{x})$ and $\boldsymbol{b}_n(\boldsymbol{x})$ to be dimensionless. In this case the slowly varying amplitude δA_n has the dimensions of a vector potential.

The sum over the subscript n in (1a) and (1b) represents a sum over frequencies ω_n. Note that all the time dependence of the fields is contained in the exponential factors; that is, the amplitudes δA_n depend only on axial distance. This representation of the field corresponds to the case in which the device is excited by a signal consisting of a discrete set of frequencies belonging to the set ω_n. It is assumed that all frequencies are integer multiples of some minimum frequency $\Delta\omega$. In this case, the nonlinear beating of any two signals in the device will produce a signal at a frequency which is a member of the set ω_n. This beating could be in the form of self beating in which case harmonic frequencies are generated, or it could be in the form of beating of two signals of different frequency generating intermodulation distortion. The restriction that members of the set ω_n are integer multiples of some minimum frequency $\Delta\omega$ can be put another way. The input signal and all other quantities of interest are assumed to be periodic in time with period $T = 2\pi/\Delta\omega$.

The time-averaged electromagnetic power flux along the structure implied by (1a) and (1b) can be evaluated using Poynting's theorem

$$P = \frac{c}{2\pi}\sum_n \left|\frac{\omega_n}{c}\delta A_n(z)\right|^2 A_{\text{eff},n} \tag{2}$$

where $A_{\text{eff},n}$ is the effective cross-sectional area defined by the relation

$$A_{\text{eff},n} = \frac{1}{2}\int d^2x_\perp\, \hat{z}\cdot(\boldsymbol{e}_n^*\times\boldsymbol{b}_n + \boldsymbol{e}_n\times\boldsymbol{b}_n^*) \tag{3}$$

and $\hat{z}$ is a unit vector in the axial direction. For a structure with slowly varying parameters, the contribution to the power flux from each frequency [i.e., each term in the sum in (2)] will be independent of axial distance in the absence of a beam or attenuation. Basically, this assumes that the parameters are tapered gently enough so that the amount of power reflected from a forward propagating wave is negligibly small. With tapering, the quantity $A_{\text{eff},n}$ will vary with axial distance as the parameters of the structure vary. Consequently, according to (2), in a structure with slowly varying parameters the amplitude δA_n will vary with axial distance even if the power flux is constant. To account for this we introduce a normalized field amplitude

$$a_n(z) = \frac{\omega_n}{c}\frac{q\delta A_n(z)}{mc^2}A_{\text{eff},n}^{1/2} \tag{4}$$

where q and m are the charge and mass of an electron, respectively. The above choice of normalization gives the following expression for the power flux:

$$P = P_{\text{flux},2}\sum_n |a_n(z)|^2 \tag{5}$$

where

$$P_{\text{flux},2} = \frac{c}{2\pi}\left(\frac{mc^2}{q}\right)^2 = 1.3862\times 10^9\,\text{W} \tag{6}$$

is a constant. A consequence of this choice of normalization is that under the stated assumptions, namely negligibly small reflection of forward propagating power, a_n varies due to attenuation and coupling to the beam, but not due to the slowly changing parameters of the structure.

The evolution of the complex amplitude is obtained by the following standard steps. Expressions (1a) and (1b) are inserted in Maxwell's equations along with the beam current. Ampere's law is dotted with $\boldsymbol{e}_n^*(\boldsymbol{x})$ and Faraday's law is dotted with $\boldsymbol{b}_n^*(\boldsymbol{x})$. The two products are combined in the same way as one forms Poynting's theorem, and the resulting expression

is averaged over the spatial period of the structure and the temporal period T of the fields. Weak attenuation is introduced by the boundary condition that the tangential electric field of the radiation does not quite vanish on the structure walls. The resulting equation for the amplitude of the nth spectral component is thus

$$\left(\frac{d}{dz}+\alpha_n(z)\right)a_n = \frac{2\pi i}{I_A A_{\text{eff},n}^{1/2}}\left\langle \int d^2x_\perp \boldsymbol{j}\cdot\boldsymbol{e}_n^*(\boldsymbol{x}) \cdot \exp\left[-i\left(\int_0^z k_{zn}(z')\,dz' - \omega_n t\right]\right]\right\rangle \tag{7}$$

where $\alpha_n(z)$ is the attenuation in Np/cm, $I_A = mc^3/q$, $\boldsymbol{j}$ is the beam current density, and the angular brackets denote averages over the temporal period of the radiation and the spatial period of the structure. The right-hand side of (7) will be further refined after a discussion of the equations of motion.

B. Equations of Motion

The beam electrons are treated as annular discs of charge of outer radius r_{bo} and inner radius r_{bi} which are constrained to move in the axial direction only. One expects this approximation to be appropriate when the electrons are confined by either a strong axial magnetic field or a system of periodic focusing magnets. The motion of the electrons will be 1-D if the frequency of the amplified signal is much smaller than the frequency of particle oscillations in the relevant confining field: the gyrofrequency or the betatron frequency. The disc approximation will be appropriate if the axial electric field of the signal does not vary appreciably over the radial extent of the electron beam.

The rate of change of electron energy is expressed in terms of the rate of change of the relativistic factor $\gamma = 1/\sqrt{1-v^2/c^2}$

$$\frac{d\gamma}{dz} = \frac{q}{mc^2}\langle\hat{z}\cdot(\boldsymbol{E}_{rf}+\boldsymbol{E}_{sc}+\boldsymbol{E}_{dc})\rangle_{\text{beam}}. \tag{8}$$

Here, $\boldsymbol{E}_{rf}$ is the electric field of the structure field given by (1a), $\boldsymbol{E}_{sc}$ is the space charge field which is discussed in part $\boldsymbol{C}$ of this section, and $\boldsymbol{E}_{dc}$ is a steady-state axial electric field, if present, which changes the energy of beam electrons as they travel through the structure. Equation (8) describes the Lagrangian rate of change of energy of a particle as it travels down the interaction region. The independent coordinate is the axial location of an electron. One must also determine the arrival time $t(z)$ of an electron at a particular axial location. This is done by solving

$$\frac{dt}{dz} = \frac{1}{v_z(\gamma)} \tag{9}$$

where the axial velocity of an electron is given in terms of the relativistic factor γ and the pitch factor Θ

$$v_z(\gamma) = c\left(1-\frac{1+(\gamma_0^2-1)\Theta^2}{\gamma^2}\right)^{1/2}. \tag{10}$$

The pitch factor Θ is the ratio of the transverse component to the total momentum on injection and γ_0 is the electron's relativistic factor on injection. It is assumed that $\Theta \ll 1$. That is, it is small enough so that the motion is 1-D, but possibly large enough that there can be a significant spread in axial velocities. In the simulations presented in the remainder of this paper, the pitch factor will be taken to be zero. This is justified for the parameters considered if the relative variation in axial velocity due to the different pitch factors is small compared with the spatial growth rate normalized to the axial wavenumber. This latter number corresponds roughly to the electronic efficiency at saturation. The initial conditions for the equations of motion are the following: particles are injected with a specified relativistic factor γ_0, pitch factor Θ, and entrance time $t(0)$. In the present simulations, the pitch factor is taken to be zero, implying a cold beam.

In the simulations, the quantity $t(z)$ is not solved directly using (9). Instead, the phase relative to the nth signal is determined. This phase is defined as

$$\psi_n = \omega_n(z/v_{z0} - t) \tag{11}$$

where v_{z0} is the initial axial velocity of a particle with pitch factor zero. The evolution of this phase is then given by

$$\frac{d\psi_n}{dz} = \omega_n(1/v_{z0} - 1/v_z). \tag{12}$$

Introduction of the phase ψ_n in the expression for the radiation field (1a) gives

$$\left.\frac{d\gamma}{dz}\right]_{rf} = \text{Re}\left\{2i\sum_n a_n(z)c_2(n,z)e^{i\psi_n}\right\} \tag{13}$$

for the contribution to the rate of change of γ due to the structure fields. In the above the quantity, $c_2(n,z)$ is defined as

$$c_2(n,z) = \frac{\langle\hat{z}\cdot\boldsymbol{e}_n\rangle_{\text{beam}}}{A_{\text{eff},n}^{1/2}}\exp\left[i\int_0^t (k_{zn}(z') - \omega_n/v_{z0})\,dz\right] \tag{14}$$

where the angular bracket denotes average over the radial extent of the beam and over one axial period of the structure fields.

The above quantity also appears effectively in (7) for the complex field amplitude. To see this, we first represent the current density in the form of a sum over moving charge discs

$$j_z(r,z,t) = \sum_j \frac{v_{z,j}(t)\delta(z-z_j(t))}{\pi(r_{bo}^2-r_{bi}^2)}\begin{Bmatrix}0, & r<r_{bi}\\ 1, & r_{bi}<r<r_{bo}\\ 0, & r>r_{bo}\end{Bmatrix}$$

where the sum is over all the electrons. Equation (7) calls for an average over one spatial period of the structure and one temporal period of the fields. Due to the time periodicity of all quantities this average may be evaluated by integration over the shaded region depicted in Fig. 1. The shaded region, a parallelogram, is preferable to a rectangle, with upper and lower boundaries at fixed t, for evaluation of the average because it contains the orbits of a group of electrons, all of

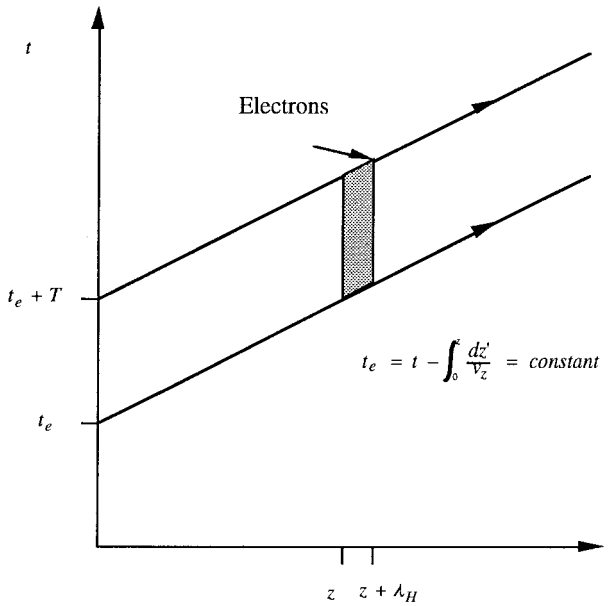

Fig. 1. Characteristics in the t versus z plane for electron trajectories. The shaded region corresponds to one spatial period of the structure and one temporal period of the fields.

which pass through both lateral boundaries. The average in (7) may be evaluated by first integrating over time

$$\sum_j \int_z^{z+\lambda_H} \frac{dz \boldsymbol{e}_n^*(\boldsymbol{x}) \cdot \hat{z}}{\lambda_H} \int_t^{t+T} \frac{dt}{T} v_{z,j}(t) \delta(z - z_j(t)) \cdot \exp\left[-i\left(\int_0^z k_{zn}(z')\, dz' - \omega_n t\right)\right] = \sum_{j'} \frac{1}{T} \int_z^{z+\lambda_H} \frac{dz \boldsymbol{e}_n^*(\boldsymbol{x} \cdot \hat{z}}{\lambda_H} \cdot \exp\left[-i\left(\int_0^z k_{zn}(z')\, dz' - \omega_n t_{j'}\right)\right]$$

where the sum over particles j' represents a sum over the group of particles entering the interaction region during one period T of time as depicted in Fig. 1, and $t_{j'}(z)$ is the time of flight for particle j' to the point z. The number of particles that will contribute to the sum is the number that entered during a time T, viz., TI/q where I is the beam current. Now the integral over z can be carried out. Because the exponent is evaluated along a particle trajectory it can be regarded as slowly varying over a distance given by the structure period λ_H. Thus, the average over z reduces to an average of the axial component of the structure field. Including the radial dependence of the current density implied by the disc model, we see that (7) calls for precisely the same average of the structure fields as does the equation of motion. The result is that the average in (7) produces

$$\left(\frac{d}{dz} + \alpha_n(z)\right) a_n = \frac{2\pi i I}{I_A} e_2^*(n,z) \langle e^{-i\psi_n} \rangle \tag{15}$$

where I is the total beam current and the angular bracket now signifies average over particles entering the interaction region during the time interval T. Since the beam current enters in the form of a ratio I/I_A, the beam current and I_A can be evaluated in any system of units. From (13) and (15), it is clear that the relevant information concerning the structure fields is contained in the complex coupling function $e_2(n,z)$. The amplitude of this quantity is related to the axial impedance. In particular

$$|e_2(n,z)|^2 = \frac{|\langle \hat{z} \cdot \boldsymbol{e}_n \rangle_{\text{beam}}|^2}{A_{\text{eff},n}} = \frac{K k_{zn}^2}{377\,\Omega} \tag{16}$$

where K is the coupling impedance in ohms. The phase of the coupling function (14) is determined by the phase velocity of the structure fields.

C. The Space-Charge Field

In this section we describe the procedure for modeling the space-charge electric field which appears in (8). The effect of this field is to resist the formation of electron bunches and, as a consequence, to give rise to collective oscillations of the beam at a modified plasma frequency. The natural frequency of these oscillations depends on the beam density, its radial profile, and the configuration of the metallic structure surrounding the beam. We assume that the basic form of the field can be written

$$\langle \hat{z} \cdot \boldsymbol{E}_{sc} \rangle_{\text{beam}} = -\sum_n \frac{4I}{\omega_n (r_{b0}^2 - r_{bi}^2)} \{ i \langle e^{-i\psi_n} \rangle R_n' + \text{c.c.} \} \tag{17}$$

where R_n' is an unknown coefficient which will be determined subsequently. Were this the only field acting on the particles, the linearized bunching factor would oscillate in time with an angular frequency ω_p, where

$$\omega_p^2 = \frac{4qIR'}{m\gamma_0^3 v_{z0}(r_{bo}^2 - r_{bi}^2)}.$$

This result is obtained by taking the small-signal limit of (8), (10), and (12) and assuming for simplicity that the beam is cold [$\Theta = 0$ in (10)]. Thus, the factor R' describes the reduction in the collective oscillation frequency accounting for the distribution of fields outside the beam.

The space-charge field is calculated including the effects of the structure using the sheath helix model. The presentation here will be different from other approaches in that no attempt will be made to separate fields into electromagnetic and electrostatic components. This approach allows one to identify in an unambiguous way the correct coefficient R' for the space-charge field to be included in the equation of motion. The space-charge field that we seek will have a time dependence similar to that of the structure fields, namely, it will be periodic in time with period T and thus include frequencies belonging to the set ω_n. In general, the number of frequencies that are needed to correctly model the space-charge term is higher than that needed to model the structure fields. This is because in the nonlinear regime the bunched current density of the beam has a high harmonic content. Frequency ω_n is generally accompanied by spatial wavenumber ω_n/v_z. These spectral components of the current will tend to excite modes of the structure over that range of frequencies where the dispersion relation of the structure is linear. However, as the excitation of the space charge field does not rely on resonance with the

structure fields, the harmonic content of the current density will produce appreciable space-charge fields over a greater range of frequencies.

The approach taken here is to assume that the beam current density is known and to calculate the total ("structure" plus "space charge") axial electric field at the beam that appears in response to the given current density. From the total field, one can then extract the appropriate factor R'. We take the form of the current density to correspond to an ensemble of moving annular discs oscillating in time with a frequency ω_n and an as yet unspecified wavenumber k_z. In order to connect the present calculation with the model of the current used in (7), we write

$$j_z(r,z,t) = \frac{I}{\pi(r_{bo}^2 - r_{bi}^2)} \exp\left[(k_z z - \omega_n t)\right] \langle e^{-i\psi}\rangle \cdot \begin{Bmatrix} 0, & r < r_{bi} \\ 1, & r_{bi} < r < r_{bo} \\ 0, & r > r_{bo} \end{Bmatrix} + \text{c.c.} \tag{18}$$

where r_{bo} and r_{bi} are the outer and inner radii of the beam discs, and the angular bracket represents the ensemble average over particles. Inserting (18) along with its corresponding charge density perturbation determined by continuity into Maxwell's equations results in the following radial differential equation for the complex amplitude of the axial electric field with frequency ω_n and wavenumber k_z:

$$\left[\frac{\partial}{r\partial r} r \frac{\partial}{\partial r} - \kappa^2\right] \tilde{E}_z(r) = \kappa^2 \frac{4I}{\omega_n(r_{bo}^2 - r_{bi}^2)} \langle e^{i\psi_n}\rangle \begin{Bmatrix} 0, & r < r_{bi} \\ 1, & r_{bi} < r < r_{bo} \\ 0, & r > r_{bo} \end{Bmatrix} \tag{19}$$

where

$$\kappa^2 = k_z^2 - \frac{\omega^2}{c^2}.$$

We solve (19) for $r < r_H$, the radius of the sheath helix. In addition, we solve the similar (but homogeneous) equation for the axial magnetic field of the TE component of the radiation for $r < r_H$. Outside the helix, $r > r_H$, we solve similar homogeneous equations for the TE and TM components of the field, but assume that a dielectric with relative permitivity ε is present. The following boundary conditions are imposed: $E_\theta(r)$ vanishes at $r = r_w > r_H$, $E_z(r)$ vanishes at $r = r_v > r_H$ (where $r_w > r_v$), simulating the effect of vanes, and the components of electric field parallel to the helix direction and surface current perpendicular to the helix direction vanish at the helix. Finally, we average the axial electric field over the annular discs. The resulting expression for this averaged field is

$$\langle E_z\rangle_{\text{beam}} = -\frac{2i\omega_n}{c^2 D(k_z,\omega_n)} I \langle e^{-i\psi}\rangle [H]^2 - \frac{4iI}{\omega_n(r_{bo}^2 - r_{bi}^2)} \langle e^{-i\psi}\rangle R. \tag{20}$$

The quantity $D(k_z,\omega_n)$ in the denominator of the first term in (20) is the vacuum dispersion function for the sheath helix

$$D(k_z,\omega_n) = \frac{\omega_n^2 r_h^2}{c^2}\left[\frac{I_0'(\kappa r_h)}{\kappa r_h I_0(\kappa r_h)} - \frac{\varepsilon C_v'(\kappa_\varepsilon r_h)}{\kappa_\varepsilon r_h C_v(\kappa_\varepsilon r_h)}\right] - \frac{1}{k_H^2 r_h^2}\left[\frac{\kappa r_h I_0(\kappa r_h)}{I_0'(\kappa r_h)} - \frac{\kappa_\varepsilon r_h D_w(\kappa_\varepsilon r_h)}{D_w'(\kappa_\varepsilon r_h)}\right] \tag{21}$$

where k_H is the helix wavenumber, D_w and C_v are linear combinations of Bessel functions

$$D_w(\kappa_\varepsilon r_h) = I_0(\kappa_\varepsilon r_h) K_0'(\kappa_\varepsilon r_w) - K_0(\kappa_\varepsilon r_h) I_0'(\kappa_\varepsilon r_w) \tag{22a}$$

and

$$C_v(\kappa_\varepsilon r_h) = I_0(\kappa_\varepsilon r_h) K_0(\kappa_\varepsilon r_v) - K_0(\kappa_\varepsilon r_h) I_0(\kappa_\varepsilon r_v) \tag{22b}$$

and

$$\kappa_\varepsilon^2 = k_z^2 - \frac{\omega^2 \varepsilon}{c^2}.$$

In (20), the quantities H and R are defined as follows:

$$H = \frac{2[\kappa r_{bo} I_1(\kappa r_{bo}) - \kappa r_{bi} I_1(\kappa r_{bi})]}{\kappa^2(r_{bo}^2 - r_{bi}^2)} \tag{23a}$$

and

$$R = 1 + \frac{2}{r_{bo}^2 - r_{bi}^2}\left\{ r I_1(\kappa r)]_{r_{bi}}^{r_{b0}} \left[r_{bo} K_0'(\kappa r_{bo}) - \frac{K_0(\kappa r_h)}{I_0(\kappa r_h)} r I_1(\kappa r)]_{r_{bi}}^{r_{bo}} \right] - r_{bi} I_1(\kappa r_{bi}) r K_0'(\kappa r)]_{r_{bi}}^{r_{bo}} \right\}. \tag{23b}$$

The first term in (20) is essentially the contribution of the structure field to the axial electric field at the beam, and the second term, involving R, is essentially the space-charge field. The quantity R is the space-charge reduction factor, and it is an interesting exercise in Bessel function identities to show that R vanishes as $r_{bi} \to r_{bo}$.

To determine the space-charge field to be inserted in (8), we write it in the form of (17) where the coefficient R_n' is to be determined. Assuming all fields vary as $\exp(ik_z z)$, the total field implied by (17) and (7) is

$$\langle \hat{E}\cdot \boldsymbol{E}_{rf} + \hat{z}\cdot \boldsymbol{E}_{sc}\rangle_{\text{beam}} = \sum_n \frac{2\pi i}{c(k_z - k_{zn})} I \langle e^{-i\psi}\rangle \frac{|z\cdot e_n|^2}{A_{\text{eff},n}} - \frac{4iI}{\omega_n(r_{bo}^2 - r_{bi}^2)} \langle e^{-i\psi}\rangle R_n' + \text{c.c.} \tag{24}$$

As can be seen, (20) and (24) have similar behavior with respect to their dependence on k_z. They both diverge as $k_z \to k_{zn}$ where k_{zn} is the solution of the vacuum dispersion relation at frequency ω_n. We pick the space-charge factor R_n' to give agreement between (20) and (24) when both are expanded about $k_z = k_{zn}$. To lowest order, the coefficient

of the singular term determines the impedance in the sheath helix model

$$\frac{Kk_{zn}^2}{377\,\Omega} = \frac{|z\cdot e_n^2}{A_{\text{eff},n}} = -\left.\frac{\pi\omega_n[H]^2}{c\partial D(k_z,\omega_n)/\partial k_z}\right|_{k_{zn}}. \quad (25)$$

In next order, matching the coefficient of the constant term gives

$$R' = R - \frac{\omega_n^2(r_{bo}^2 - r_{bi}^2)D_s''}{4c^2(D_s')^2} \quad (26)$$

where

$$D_s' = \left.\frac{\partial(D/H^2)}{\partial k_z}\right|_{k_{zn}}$$
$$D_s'' = \left.\frac{\partial D_s'}{\partial k_z}\right|_{k_{zn}}. \quad (27)$$

The difference between R and R' can be interpreted as the effect of the sheath helix on the space-charge reduction factor. In particular, if the helix is replaced by a conducting tube, no structure field can resonate with the beam, and the space-charge reduction factor is simply R. With the helix present, some of the space-charge field is able to penetrate outside the helix, and the reduction factor is modified.

The final equation of motion is thus

$$\frac{d\gamma}{dz} = \text{Re}\left\{2i\sum_n a_n(z)e_2(n,z)e^{i\psi_n} - \frac{8Ii}{I_A(r_{bo}^2 - r_{bi}^2)|}\cdot\sum_{n'}\frac{cR_{n'}'}{\omega_{n'}}e^{i\psi_{n'}}\langle e^{-i\psi_{n'}}\rangle\right\} + \frac{q}{mc^2}\langle\hat{z}\cdot\boldsymbol{E}_{dc}\rangle_{\text{beam}} \quad (28)$$

where the separate sums over n and n' are over frequencies belonging to the set ω_n. In our model, the number of frequencies kept to evaluate the space-charge term is independent of the number kept to evaluate the structure fields. In particular, a range of frequencies is specified in the input list for the radiation field as is the number of space-charge harmonics. In computing the space-charge factor R_n' for each frequency harmonic, the simulation code first checks to see if the frequency is in the range corresponding to the structure fields. If it is, the reduction factor is calculated according to (30). If the space-charge harmonic frequency is out of the range specified for the structure fields, the reduction factor is taken to be just R and calculated for a spatial wavenumber $k_z = \omega_n/v_{z0}$.

D. Nonlinear Dielectrics

To treat the effect of nonlinear dielectric elements, we assume that the nonlinearity is weak in the sense that the signal field is still described by (1a) and (1b), but the nonlinearity modifies the wave equation (7). Effectively, we separate the current density $\boldsymbol{j}$ into a contribution from the electron beam, calculated as described above, and a contribution from the nonlinearity of dielectrics in the vicinity of the structure. The linear contribution of these dielectrics is included implicitly in the determination of the transverse eigenfunctions $\boldsymbol{e}_n$ and $\boldsymbol{b}_n$. The nonlinear dielectric contribution to the current density is given by $\boldsymbol{j} = \partial\boldsymbol{P}/\partial\boldsymbol{t}$, where $\boldsymbol{P}(t)$ is the nonlinear polarization. The polarization can be expressed in terms of the instantaneous electric field $4\pi\boldsymbol{P}(t) = \delta\varepsilon^{(3)}|\boldsymbol{E}(t)|^2\boldsymbol{E}(t)$ where $\delta\varepsilon^{(3)}$ is a constant characterizing the nonlinear response of the dielectric, and we have assumed the dielectric responds instantaneously to the electric field. Inserting the above into (7) and introducing the normalized amplitudes $a_n(z)$ defined in (4) results in the following evolution equation for the nth mode:

$$\frac{d}{dz}a_n = \frac{\omega_n}{2c}\int d^2x_\perp\left\langle\delta\varepsilon(t)\frac{e^{-i\phi_n}\boldsymbol{e}_n^*(\boldsymbol{x})}{A_{\text{eff},n}^{1/2}}\cdot\sum_m\left[\frac{ie^{i\phi_m}\boldsymbol{e}_m(\boldsymbol{x})a_m}{A_{\text{eff},m}^{1/2}} + \text{c.c.}\right]\right\rangle \quad (29)$$

where

$$\delta\varepsilon(t) = \delta\varepsilon^{(3)}\left(\frac{mc^2}{q}\right)^2\left|\sum_m\left[\frac{ie^{i\phi_m}\boldsymbol{e}_m(\boldsymbol{x})a_m}{A_{\text{eff},m}^{1/2}} + \text{c.c.}\right]\right|^2$$

is the time dependent nonlinear contribution to the dielectric constant, and $\varphi_n = \int_0^z k_{zn}(z')\,dz' - \omega_n t$ is the phase of the nth signal component. It is understood that the right-hand side of (29) is to be added to (7).

The angular brackets in (29) indicate that the time-dependent quantity is to be averaged over the repetition time $T = 2\pi/\Delta\omega$. In general, this induces a nonlinear coupling between all signal components. If only a single frequency is present, (29) gives rise to a nonlinear wavenumber shift δk_z

$$\delta k_{zn} = \frac{3\omega_n}{2c}\left(\frac{mc^2}{q}\right)^2|a_n|^2\int d^2x_\perp\delta\varepsilon^{(3)}\frac{|\boldsymbol{e}_n(\boldsymbol{x})|^4}{A_{\text{eff},n}^2}. \quad (30)$$

The sign of the wavenumber shift depends on the sign of the coefficient $\delta\varepsilon^{(3)}$. We shall find that a negative wavenumber shift, giving a negative phase shift when integrated over the length of the region where the nonlinear dielectric is located, is required to compensate the positive nonlinear phase shift of the electron beam. Note that $\delta\varepsilon^{(3)}$ depends both on transverse and axial coordinates. Thus, the wavenumber shift given by (30) could be an arbitrary function of z, reflecting the placement of the dielectric elements along the interaction region. In fact, these elements need not be in the interaction region, but could be anywhere in the signal path.

To estimate the degree to which various modes are affected by the nonlinear dielectric, we temporarily assume that the perturbed dielectric constant $\delta\varepsilon(t)$ is independent of time and can be factored into the product of a magnitude $\delta\varepsilon_0$ and a spatially dependent form factor $\delta\varepsilon(\boldsymbol{x}_\perp)/\delta\varepsilon_0$. In this case it induces a linear phase shift for each mode given by

$$\delta k_{zn,L} = \frac{\omega_n}{2c}\tau_n^2\delta\varepsilon_0 \quad (31)$$

where the dimensionless parameter τ_n characterizes the overlap between the perturbed dielectric and the mode electric field

$$\tau_n^2 = \int d^2x_\perp\frac{\delta\varepsilon(\boldsymbol{x}_\perp)}{\delta\varepsilon_0}\frac{|\boldsymbol{e}_n(\boldsymbol{x}_\perp)|^2}{A_{\text{eff},n}}. \quad (32)$$

This parameter is estimated in the present model by assuming the nonlinear dielectric fills the entire region between the wall and the helix, just as the support structure for the helix is modeled in the sheath helix approximation as a uniform dielectric annulus. Thus, τ_n can be determined by differentiation of the solution of the sheath helix dispersion relation with respect to the dielectric constant in the outer region

$$\tau_n^2 = \frac{2c}{\omega_n}\frac{\partial k_{zn}}{\partial \varepsilon}. \tag{33}$$

Finally, our expression for the nonlinear phase shift in the presence of many signals is written

$$\frac{d}{dz}a_n = \frac{\omega_n}{2c}\left\langle \delta\varepsilon_0(t)\tau_n e^{-i\phi_n}\cdot\sum_m [i\tau_m e^{i\phi_m}a_m + \text{c.c.}]\right\rangle \tag{34}$$

where

$$\delta\varepsilon(t) = \delta\varepsilon_0^{(3)}A_\varepsilon(z)\left(\frac{mc^2}{q}\right)^2\left|\sum_m [i\tau_m e^{i\phi_m}a_m + \text{c.c.}]\right|^2 \tag{35}$$

and $\delta\varepsilon_0^{(3)}$ is the magnitude of the nonlinear dielectric coefficient and $A_\varepsilon(z)$ is the effective cross-sectional area of the nonlinear dielectric element. In the case of single-frequency operation, (34) and (35) predict a nonlinear wavenumber shift

$$\delta k_{zn} = \frac{3\omega_n}{2c}\left(\frac{mc^2}{q}\right)^2|a_n|^2\delta\varepsilon_0^{(3)}A_\varepsilon\tau_n^4 \tag{36}$$

which can be compared with (30), thus giving the definition of the effective area.

While it seems that many simplifying assumptions and unknown form factors have been introduced to describe the effect of the nonlinear dielectric, this effect depends only on the integrated nonlinear phase shift induced by the signal. Thus, while a specific realization is dependent on details such as the coupling parameters τ_n, the effective area $A_\varepsilon(z)$, and the magnitude of the nonlinear coefficient $\delta\varepsilon_0^{(3)}$, once these are selected to give a specific phase shift the operation of the device should be well described by (34) and (35).

III. Reduction of Intermodulation Distortion

We begin our discussion of intermodulation distortion by considering the nonlinear transfer function for single-frequency operation of a TWT amplifier. Suppose a signal at a single frequency ω_n with complex amplitude $a_n(0)$ is injected into the amplifier. As the phases of injected electrons are uniformly distributed, the phase of the amplified signal at any point along the interaction region is related to the phase of the injected signal by an additive constant which depends only on the magnitude of the injected signal. Further, the magnitude of the signal at any point along the interaction region only depends on the magnitude of the injected signal. Thus, the nonlinear gain of the TWT can be characterized by a complex transfer function

$$g_n(|a_n(0)|) = a_n(L)/a_n(0)$$

where L is the length of the interaction region.

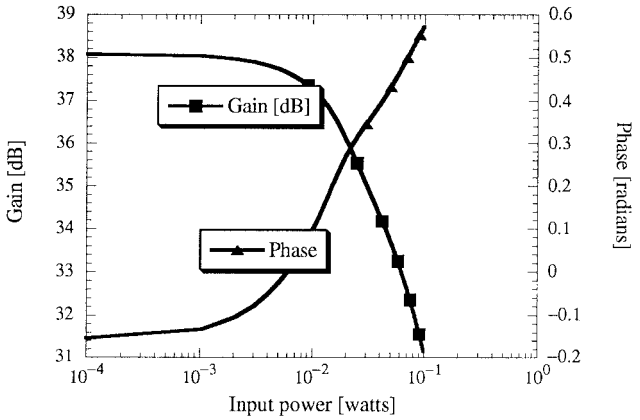

Fig. 2. Gain and phase of the nonlinear transfer function versus input power for a TWT with the parameters shown in Table I.

TABLE I
Low Dispersion Structure Parameters

Helix period, λ_H	0.07.779 cm
Helix radius, r_H	0.12446 cm
Wall radius, r_w	0.2794 cm
Vane radius, r_v	0.19 cm
Effective dielectric constant, ε	1.25
Beam voltage, V_B	2.84 kV
Beam current, I	0.17 A
Beam radius, r_{bo} (r_{bi} = 0.)	0.05 cm

As mentioned, the transfer function is complex. Its magnitude and phase both depend on the amplitude of the injected signal. This is illustrated in Fig. 2, where we plot the magnitude and phase of the transfer function at 5 GHz for a structure with parameters given in Table I. These parameters are similar to, but not identical to, those of the Northrop Grumman research tube #8. In the plot, the magnitude of the transfer function is given in decibels, and the magnitude of the input signal is given in units of power. As input power is increased, two effects are apparent. First, the gain decreases as the amplifier is driven to saturation. This is known as gain compression. Second, the phase of the transfer function increases with signal power. This is known as amplitude modulation (AM) to phase modulation (PM) distortion. Changing parameters of the amplifier, for example the beam voltage [12], or introducing dynamic velocity tapering [13] can reduce the amount of gain compression considerably. However, these measures have substantially less influence on the phase distortion. The fundamental reason for the phase distortion is the dependence of the beam speed on the signal amplitude. In a TWT, the signal is partially carried by the electromagnetic slow wave and partially carried by the streaming electron beam. The phase delay associated with the beam is $\int_0^L dz\omega_n/v_z$. Note that this phase is positive as a consequence of our choice of representation of the complex fields in (1a) and (1b). Thus, at high signal levels, when the beam loses substantial energy and slows down, the phase delay associated with the beam goes up.

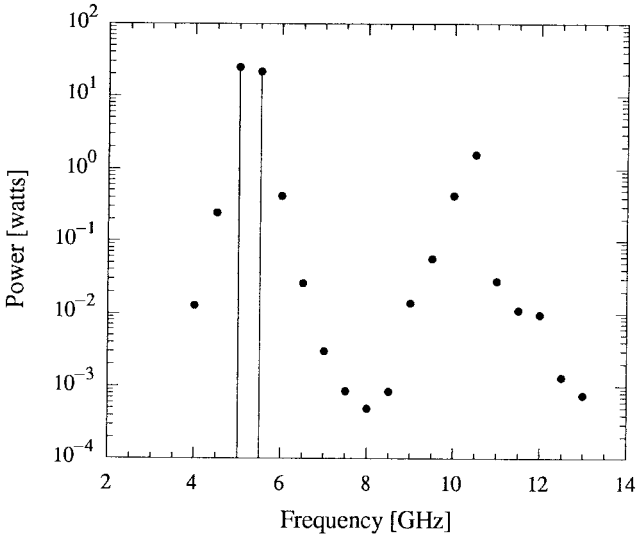

Fig. 3. Output power versus frequency for the TWT of Table I. The two vertical lines correspond to the frequencies of the injected signals.

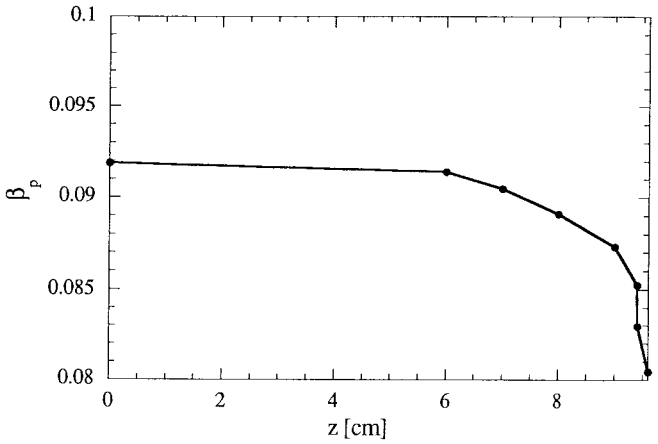

Fig. 4. Profile of normalized phase velocity versus axial distance for optimized circuit.

The effect of the nonlinearity of the transfer function when multiple signal frequencies are present is illustrated in the output power spectrum of Fig. 3. In this case, we have injected two signals of equal power (4 mW), one at 5 GHz and one at 5.5 GHz. The output spectrum consists of all frequencies separated by 0.5-GHz intervals. From the figure is seen that for frequencies near the driven signals the largest power is in the third-order intermodulation products at 4.5 and 6 GHz, respectively. There is also signal power at frequencies corresponding to the second harmonics and sum of the driven signals.

The goal of our study is to reduce the amplitude of the intermodulation products. This will be done by finding ways to improve the linearity of the transfer function. The ideal transfer function would be one in which the complex gain is independent of the injected signal amplitude. Use of predistortion linearizers attempts to reach this goal by passing the signal first through a nonlinear circuit which compensates for gain compression and phase distortion. We instead will use a combination of dynamic velocity taper and nonlinear phase modification to linearize the tube. To be specific, we take the circuit parameters listed in Table I as a starting point. We then add a region of nonlinear dielectric with wavenumber shift given by (34) to the last 0.2 cm of the interaction region. In fact, this nonlinear phase shifter could equally well be attached outside the tube. To implement dynamic velocity taper, we allow the helix wavelength to be a piecewise-linear function of axial distance defined at eight points along the interaction region: $z_i = 0.0$, 6.0, 7.0, 8.0, 9.0, 9.4, 9.41, and 9.6 cm. The nonlinear transfer function then depends parametrically on the eight values of helix period, λ_{Hi} for $i = 1$–8, and the strength of the dielectric nonlinearity $\delta\varepsilon_0^{(3)}$

$$g_n = g_n(|a_n(0)|; \lambda_{Hi}, \delta\varepsilon_0^{(3)}).$$

The degree of linearity is quantified by the square error which we define to be

$$\text{error}\,(\lambda_{Hi}, \delta\varepsilon_0^{(3)}) = \int_o^{P_{\max}} \frac{dP_{\text{out}}}{P_{\max}} \left| \frac{g_n(|a_n(0)|) - g_n(0)}{g_n(0)} \right|^2. \tag{37}$$

Thus, a perfectly linear amplifier, over the range of output powers $P_{\text{out}} < P_{\max}$ would produce zero error. The error defined in (37) is then minimized numerically with respect to the parameters, λ_{Hi} and $\delta\varepsilon_0^{(3)}$. For the circuit under consideration, there is considerable excitation of the second harmonic. Thus, the nonlinear transfer function is calculated including the excitation of the second harmonic signal.

The results of the minimization of the gain error for the case of 60-W maximum output power are displayed in Figs. 4–8. First, in Fig. 4 we display the optimum profile of axial phase velocity. This profile is very similar to one which results in optimum efficiency. By way of comparison, the error value for the untapered uncompensated circuit is 2.42×10^{-2} whereas the tapered phase-compensated circuit is 3.66×10^{-5}.

Fig. 5 shows a comparison of the gain compression for the compensated and optimized transfer function and the original transfer function displayed in Fig. 2, except here the transfer function is plotted versus output power. Clearly, the improvement in the linearity is particularly evident in the dependence of the phase of the transfer function on output power. For further comparison, Fig. 5 also displays the transfer function obtained when the nonlinear phase compensation is not employed but the circuit parameters are chosen to minimize the error defined in (37). This case shows only a very modest improvement over the unlinearized case and is not clearly as effective as the combination of phase compensation and circuit tapering. Fig. 6 shows the output spectra for the linearized and unlinearized amplifiers when two signals are injected. In this case, the signal levels have been adjusted so that the output power is 30 W in each case. For these parameters there is over an order of magnitude reduction in power in the intermodulation products in the optimized and phase-compensated case. The role of the nonlinear dielectric's in reducing the intermodulation product amplitudes is illustrated in Fig. 7. Here we have plotted the power in the two driven signals, 5.0 and 5.5 GHz, as well as the power in the third-order intermodulation products at 4.5 and 6.0 GHz. Only the last 0.6 cm of the interaction region as shown; the shaded region corresponds to where the nonlinear dielectrics are present. It can be seen that the intermodulation power

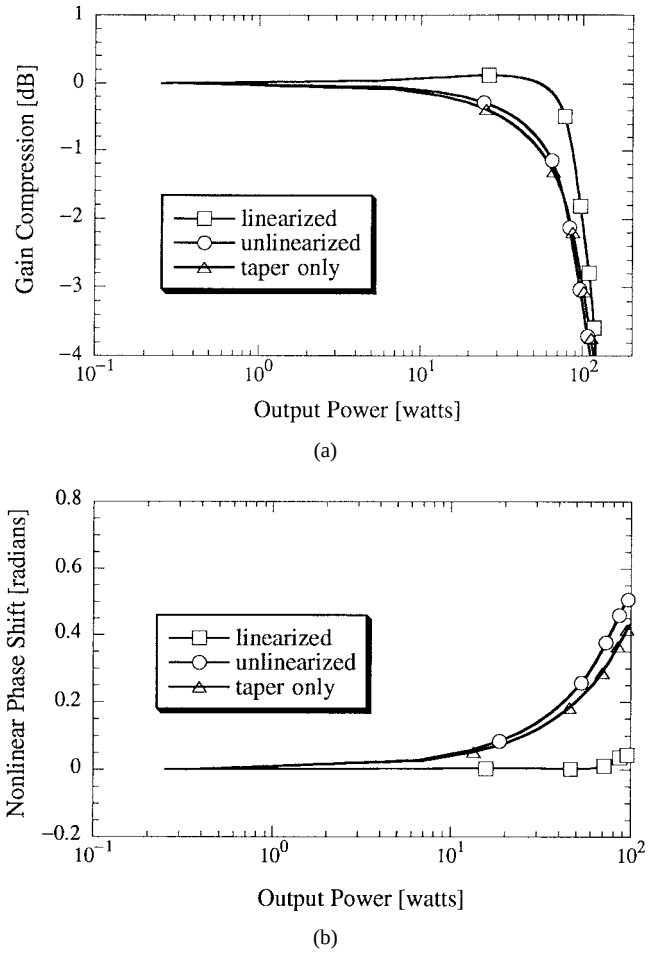

Fig. 5. Comparison of (a) gain compression and (b) phase distortion for linearized, unlinearized, and taper-optimized circuits.

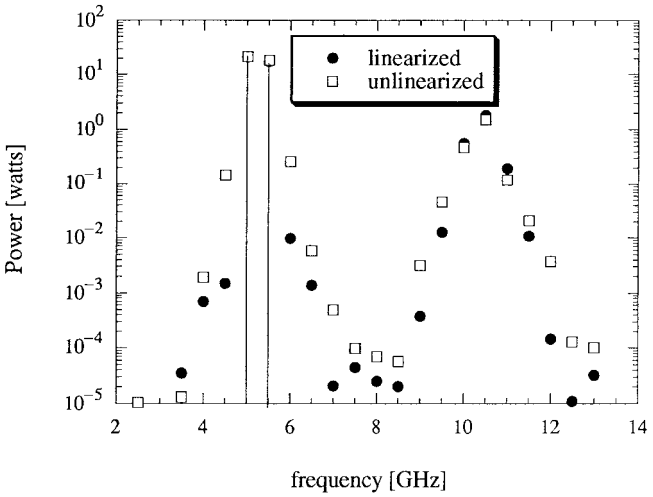

Fig. 6. Comparison of output spectra for linearized and unlinearized circuits.

is reduced dramatically in this region. We note that this is not attenuation, rather the power from the intermodulation products is converted into power at the driven frequencies.

The effectiveness of the linearization over a range of output powers is illustrated in Fig. 8 where we have plotted the signal to intermodulation power ratio as a function of output power.

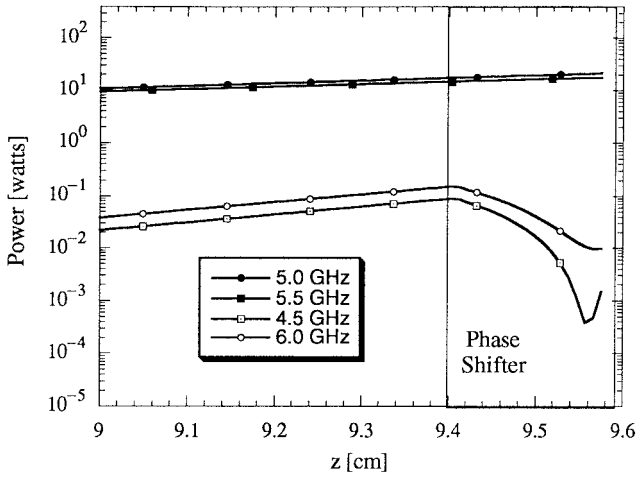

Fig. 7. Power versus axial distance for the linearized circuit. The injected signals are at 5.0 and 5.5 GHz. The shaded region corresponds to the location of the nonlinear dielectric element.

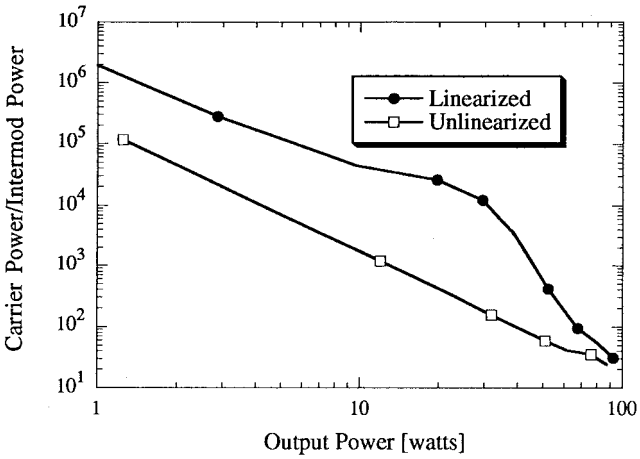

Fig. 8. The ratio of power in the driven signals to power in the third-order intermodulation products as a function of output power for the linearized and unlinearized circuits.

This ratio is one to two orders of magnitude higher for the linearized case for powers below 40 W. At higher powers, approaching the saturated output power of the device the ratio decreases. The unlinearized case shows the expected $(P_{\rm out})^{-2}$ dependence. The linearized case shows this dependence at low output powers, with a slight improvement in the range of powers for which the optimization was performed. The location of this enhancement can be varied by changing the value of $P_{\rm max}$ in the optimization. For the present case, if one requires a signal to intermodulation distortion ratio of 10^4, then the linearized case allows for operation with over six times the output power.

In the preceding we have compared the unlinearized circuit with one in which nonlinear dielectric elements are added at the output end of the interaction region. We now compare the case in which the nonlinear dielectric element is placed at the input with the case in which it is placed at the output. In the case of input linearization we again perform the optimization over the helix period and the nonlinear dielectric constant.

In this way, the performance predicted with input linearization should be comparable to what is achieved with

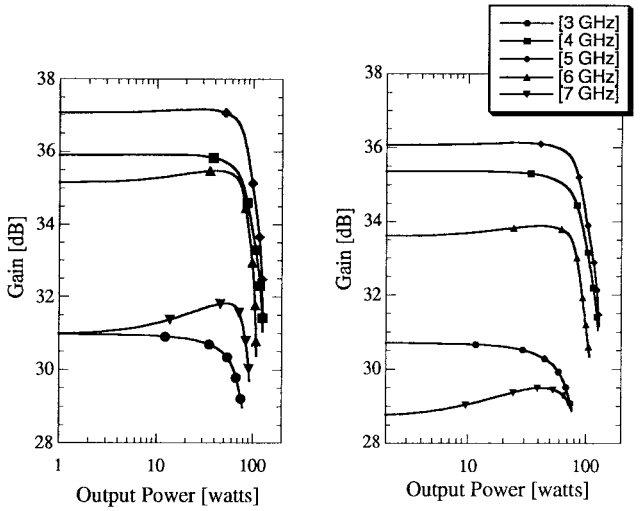

Fig. 9. Gain versus output power for a range of drive frequencies for (a) output linearization and (b) input linearization.

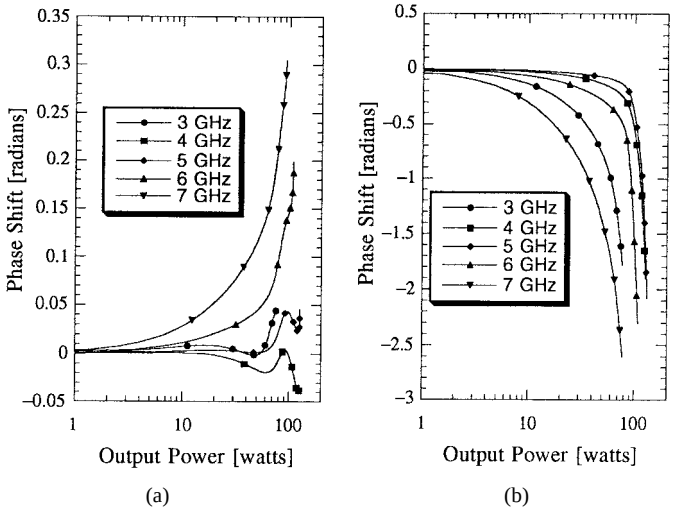

Fig. 10. Phase shift versus output power for a range of drive frequencies for (a) output linearization and (b) input linearization.

predistortion linearizers. We perform the optimization for $P_{\max} = 60$ W and frequency 5 GHz. We then compare the nonlinear transfer functions for a range of drive frequencies. This comparison is illustrated in Figs. 9 and 10 where the transfer functions for the cases of output linearization and input linearization are shown receptively. In Fig. 9, which shows the gain versus output power, there is not much difference between the two cases. However, Fig. 10, which shows the phase versus output power, is more revealing. As is seen, the linearization which is optimized for 5 GHz is more effective over a range of frequencies for the output linearization case as compared with the input linearization case. Note that the scales on these two figures differ, and that the variation of phase with output power is much smaller in the output linearization case. This is further illustrated in Fig. 11 where we compare the carrier to intermodulation distortion power as a function of frequency for two methods. To generate this plot, two signals of equal power are injected, one at the indicated frequency, and one at

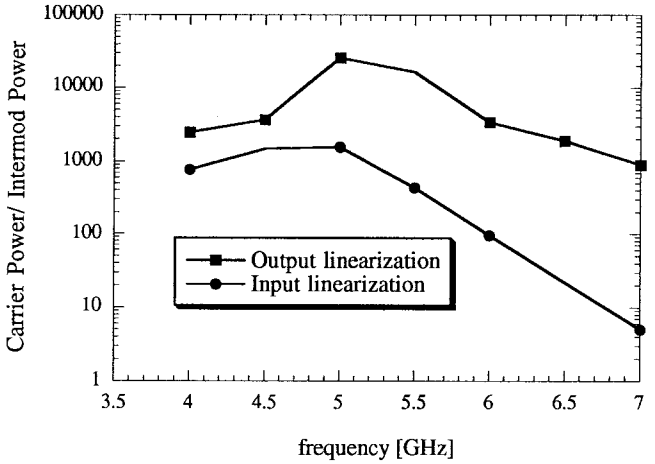

Fig. 11. Comparison of carrier to intermodulation power as a function of frequency for the cases of input and output linearization.

a frequency 0.5 GHz higher. The power in the injected signals is adjusted so that the output power is 30 W. We then plot the ratio of the power in the two driven frequencies with that in the two third-order intermodulation products. We note that even at 5 GHz where both circuits were optimized, the output linearized circuit has superior linearity as compared with the input linearized circuit. This difference grows as frequency is varied away from 5 GHz. The main cause for this difference is that the distortion in the TWT is generated at the output where the signal is large. Thus, the level of the output power is a more reliable indicator of the distortion than the input power. We conclude that output linearization is an effective way to reduce intermodulation distortion in a TWT amplifier, and the reduced distortion can be realized over a range of operating frequencies. Fig. 11 shows, for example, that the carrier to intermodulation power ratio remains well over 10^3 for frequencies 4 and 6.5 GHz.

IV. Electronic Tuning of Gain

In this section, we consider the possibility of tuning the frequency response of the TWT transfer function by electrically varying the dielectric constant of the rods which support the helix. The basic idea is that these rods could be made of or coated with a ferroelectric material (operating in the paraelectric phase). A dc voltage applied to the rods would then change their dielectric constant and alter both the phase velocity and coupling impedance of the helix structure. We imagine that relatively modest changes, $\pm 20\%$, are realizable and seek to determine the effect on the TWT transfer function. The bandwidth of helix TWT's is determined by both the dispersion of the structure as well as the frequency dependence of its coupling impedance. For this reason, we cannot employ the formulation of Section II-C to calculate the effect of a small change in dielectric constant on the transfer function. This formulation calculates only the change in dispersion (specifically, axial wavenumber) due to a given change in dielectric constant. Instead, we use the solutions of the sheath helix dispersion relation (25) and vary the dielectric constant of the outer region.

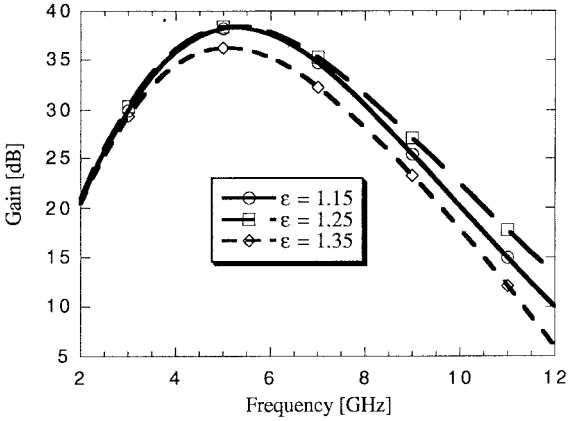

Fig. 12. Gain versus frequency for the low dispersion structure of Table I.

TABLE II
HIGH DISPERSION STRUCTURE PARAMETERS

Helix period, λ_H	0.0802 cm
Helix radius, r_H	0.12446 cm
Wall radius, r_w	0.18 cm
Vane radius, r_v	0.2794 cm
Effective dielectric constant, ε	1.75
Beam voltage, V_B	3.0 kV
Beam current, I	0.17 A
Beam radius, r_{bo} ($r_{bi} = 0.$)	0.05 cm

We begin this study by calculating the linear gain as a function of frequency for the untapered structure considered in the previous section. The parameters of this structure are shown in Table I. Fig. 12 shows the gain versus frequency for this structure when the effective dielectric constant is varied.

As can be seen, the main effect of varying the dielectric constant is to vary the magnitude of the gain but not to vary the frequency of maximum gain. This is because the structure has low dispersion. Thus, varying the dielectric constant mainly moves the phase velocity on and off synchronism with the beam across the entire frequency range. Further, since the effective dielectric constant is rather low, $\varepsilon = 1.25$, the variation in susceptibility $(\varepsilon - 1)$ implied by Fig. 12 is rather large.

To achieve tuning requires a dispersive phase velocity. Additionally, the gain at higher frequencies tends to be limited by the decrease in coupling impedance. Thus a means must be found to increase coupling impedance at higher frequency. The structure whose parameters are given in Table II has these properties. Note that for this structure the vane radius is greater than the wall radius. This implies that the interaction waveguide needs to be loaded with conducting discs. Future studies which go beyond the sheath helix model will address the issue of the structure geometry in more detail.

The dispersion and coupling impedance versus frequency for the two structures is shown in Figs. 13 and 14. As can be seen, the phase velocity for the high dispersion structure varies across the frequency band, and the coupling impedance

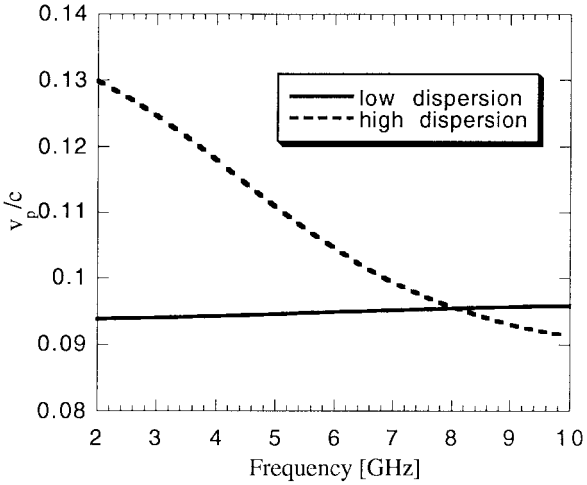

Fig. 13. Comparison of phase velocities for low- and high-dispersion structures. Parameters are given in Tables I and II.

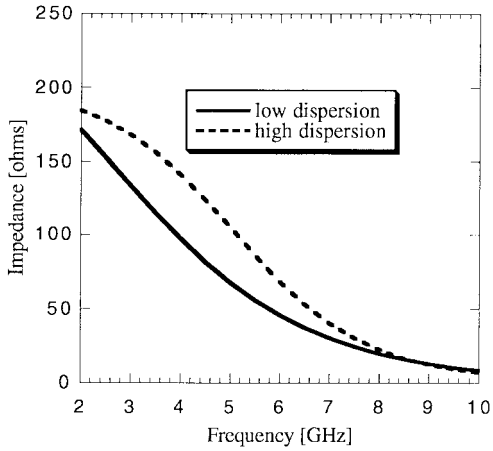

Fig. 14. Comparison of coupling impedance for low- and high-dispersion structures. Parameters are given in Tables I and II.

for frequencies between 5 and 7 GHz is 30%–50% larger than that of the low-dispersion structure.

The gain versus frequency for the high-dispersion structure is shown for several values of dielectric constant in Fig. 15.

In the case of Fig. 15, variation of the dielectric constant has tuned the frequency of peak gain from 5 to 8 GHz. Further, the overall bandwidth has been improved over the low-dispersion structure. While the improvement in bandwidth over the low-dispersion case is marginal, it must be remembered that a helix TWT is an inherently high-bandwidth device. Thus, it is difficult to improve the bandwidth by a large margin. The concept of electronic tuning of gain to increase bandwidth might be more attractive if applied to low-bandwidth amplifiers, such as coupled-cavity TWT's.

V. CONCLUSIONS

In this paper, we have examined two possible uses for nonlinear dielectric elements in traveling-wave tube amplifiers. The realization of these depends in large part on finding appropriate dielectric materials. The two schemes require materials for which the dielectric constant depends on the strength of the

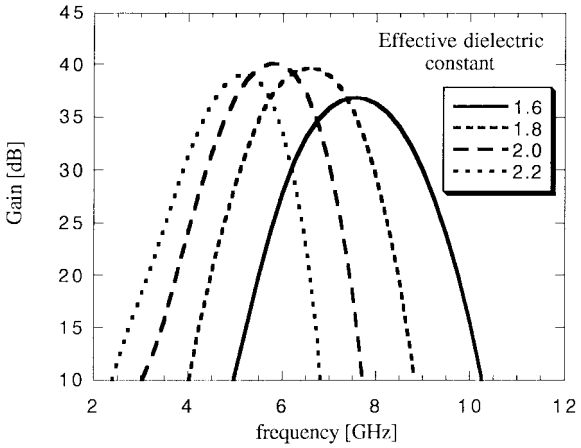

Fig. 15. Gain versus frequency for t several values of dielectric constant for the structure whose parameters are given in Table II.

applied electric field. In the case of intermodulation distortion reduction, what is required is a material with a negative coefficient of third-order dielectric constant $\delta\varepsilon_0^{(3)}$. While in the case of electronically tuning of amplifier gain what is required is a material whose first-order dielectric constant can be varied by applying a bias voltage.

A possible candidate material fulfilling both requirements is a ferroelectric operating above the Curie temperature. These materials have a dielectric constant which depends on the applied electric field. For small electric fields, the dielectric constant depends quadratically on the field strength and decreases with increasing field strength giving the required negative third-order dielectric constant [14]. Additionally, the dielectric constant can be changed over a relatively large range by varying a dc bias electric field, this feature is required for the concept of electronically tuning the gain of a TWT. Recent advances in the development of barium strontium titanate composites [15] have allowed significant progress in the design of phase shifters for phased array antennas. The proper composition of barium and strontium with additives allows one to operate the phase shifter in the para-electric regime, thus reducing possible losses and hysteresis effects. For example, these material improvements have resulted in voltage-controlled phase shifts greater than 360 degrees with less than 6-dB insertion loss [16]. The phase-shift variation is proportional to the tunability of a material $[\varepsilon'(0)-\varepsilon'(V_{\rm app})]/\varepsilon'(0)$, where $\varepsilon'(0)$ is the dielectric constant without applied electric field and $\varepsilon'(V_{\rm app})$ is the dielectric constant after some electric field is applied. Depending on the material composition the tunability can be between 1%–40% [17] when the electric field on the order of few volts/mm is applied. The dielectric constant of these materials can be as high as several thousand. The loss tangent also has significant variation as a function of compositions as well as a function of frequency. For example, at 10 GHz $Ba_{0.50}Sr_{0.50}TiO_3$ with 60% by weight added oxide has a relative permitivity 84.5 and loss tangent 6.55×10^{-3} [15].

As mentioned, an important consideration for such materials is the amount of loss caused by their introduction into the circuit. For example, in the case of output linearization, since the phase compensation is applied at the output of the amplifier it is critical that the loss be small. An order of magnitude estimate of these losses can be obtained as follows. Examination of Fig. 5(b) shows that the nonlinear dielectric element must provide a nonlinear phase shift of about 0.4 rad to be effective. This number is obtained by comparing the phase shift at 100-W output power in the taper optimized circuit with that in the fully linearized circuit. This phase shift would be realized by passing the signal through a section of circuit of length L_ε which had a nonlinear wavenumber shift of the form given by (30). Using the same reasoning that led to (33), we can write this phase shift $\delta\phi = \delta\varepsilon_{nl}(\partial k_{zn}/\partial\varepsilon)L_\varepsilon$ where $\delta\varepsilon_{nl}$ is the nonlinear shift in the dielectric. The attenuation Γ in decibels realized in passing through this dielectric, assuming perfect matching, can be expressed in terms of the loss tangent and the real part of the dielectric constant, $\Gamma = 8.69(\tan\delta)\varepsilon'(\partial k_{zn}/\partial\varepsilon)L_\varepsilon$. Thus, for a phase shift of 0.4 rad, the attenuation can be estimated as

$$\Gamma = 3.48(\tan\delta)(\varepsilon'/\delta\varepsilon_{nl}). \tag{38}$$

This attenuation will be small provided the loss tangent is much smaller than the tunability of the material $\delta\varepsilon_{nl}/\varepsilon'$. For example, it is reasonable to assume 10% tunability and 1% loss tangent is achievable in practice. This will result only in 0.348-dB attenuation. The above estimate, however, assumed perfect matching. The dielectric constant of ferroelectric materials operating in this regime tends to be very large. Thus, there is the problem, which is solvable with proper matching design, of coupling the field into the dielectric without inducing large reflections.

The issue of reflections is also important from the point of view of device stability. If the nonlinear dielectric section is placed at the output of the device, reflections would have to be kept below a prescribed level to avoid unwanted oscillations. Addition of a circulator between the amplifier and the nonlinear element could mitigate against the effect of reflections. If the dielectric is placed in the device, different considerations come into play. The linear susceptibility of the material would effect the phase velocity of the wave in the section of the interaction region where the nonlinear dielectric is added. This would have to be taken into account in designing the structure so that the phase velocity had the desired value in each section of the interaction region. Once this has been achieved the reflections from the nonlinear response of the dielectric material are quite small as these only shift the phase of the forward wave by a small amount. The problem would be in finding a design in which the linear and nonlinear response of the dielectric was matched to the requirements of prescribed phase velocity and nonlinear phase shift.

The electronic tuning of gain can be implemented, for example, by incorporating the ferroelectric material in the dielectric structures which are used in the TWT circuit to support the helix. If the amplifier is of the coupled-cavity type the ferroelectric material would be added to the individual cavities of the structure. The dielectric constant of the ferroelectric material is typically measured in thousands, while the dielectric constant of BeO, the material of which the helix support structures is made, is about 6. The high dielectric

constant will again raise the issue of coupling the fields into the material. One approach would be to deposit a very thin layer of the ferroelectric material on to another dielectric substrate. Electrical conductors would have to be attached so that a dc electric field would be applied to the ferroelectric material. If the dimension of the ferroelectric is small enough it would only require a small voltage to achieve the desired tunability. In future studies we will address more specifically the optimum geometry and effective implementation of the adaptive TWT circuit with a tunable ferroelectric for gain control.

What we have shown here is that nonlinear dielectric elements have, in principle, the capability of enhancing the performance of TWT amplifiers. The next step is to attempt to implement these ideas in a real amplifier.

REFERENCES

[1] A. S. Gilmour, *Principles of Traveling Wave Tubes*. Norwood, MA: Artech House, 1994.
[2] H. Seidel, "A microwave feed-forward experiment," *Bell Syst. Tech. J.*, vol. 50, no. 9, pp. 2879–2916, 1971.
[3] S. Narahashi and T. Nojima, "Extremely low distortion multi carrier amplifier—Self adjusting feed forward amplifier," CH2984-3/91/0000-1991, IEEE, pp. 1485–1490.
[4] H. G. Kosmahl, "Modern multistage depressed collectors—A review," *Proc. IEEE*, vol. 70, pp. 1325–1334, 1982.
[5] A. Katz, R. Sudarsanam, and D. Aubert, "A reflective diode linearizer for spacecraft applications," in *IEEE MTT-S Int. Microwave Symp. Dig.*, June 1985, pp. 661–664.
[6] J. Maynard, B. Cogo, and M. Pouysegur, "Fully MMIC Ku-band and C-band CAMP/linearizers for TWT's," European Space Agency WPP-072, Space TWTA's Workshop, Noordwijk, The Netherlands, May 18–20, 1994.
[7] A. Adler, private communication, June 1997.
[8] T. Antonsen, Jr., and B. Levush, "CHRISTINE: A multifrequency parametric simulation code for traveling wave tube amplifiers," NRL/FR/6840-97-9845.
[9] J. E. Rowe, *Nonlinear Electron-Wave Interaction Phenomena*. New York: Academic, 1965.
[10] A. J. Giarola, "A theoretical description for the multiple-signal operation of a TWT," *IEEE Trans. Electron Devices*, vol. ED-15, p. 381, 1968.
[11] N. J. Dionne, "Harmonic generation in octave bandwidth traveling-wave tubes," *IEEE Trans. Electron Devices*, vol. ED-17, p. 365, 1970.
[12] S. Wallander, "Non-linear multi-signal traveling wave tube theory," *Int. J. Electron.*, vol. 29, p. 201, 1970.
[13] H. Kosmahl and J. Peterson, "A TWT amplifier with a linear power transfer characteristic and improved efficiency," presented at AIAA's 10th Communications Satellite Systems Conference, Orlando, FL, Mar. 18–22, 1984, NASA Tech. Memo. 83590.
[14] O. Vendik, "Dielectric nonlinearity of the dispacive ferroelectrics at UHF," *Ferroelectrics*, vol. 12, pp. 85–90, 1976.
[15] R. G. Geyer, J. Krupka, L. Sengupta, and S. Sengupta, "Microwave properties of composite ceramic phase shifter materials," in *IEEE Proc. Int. Symp. Application of Ferroelectrics, 96*, 1996, pp. 851–854.
[16] R. Babbitt, T. Koscica, W. Drach, and L. Didomenico, "Ferroelectric phase shifters and their performance in microwave phased array antennas," *Integ. Ferroelect.*, vol. 8, pp. 65–76, 1995.
[17] L. Sengupta, E. Ngo, S. Stowell, M. O'Day, and R. Lancto "Processing, packaging, and characterization of electroceramic materials for phased array antennas," ARL-TR-448, May 1994.

Thomas M. Antonsen, Jr., (M'87), for a biography, see this issue, p. 425.

Baruch Levush (M'88–SM'90), for a biography, see this issue, p. 415.